SUPPORTING INFORMATION

Note: we have 21 Supplemental Figures, 3 Supplemental Tables, 1 Supplemental Methods file, 1 Supplemental Data Set legends file and 5 Supplemental Data Set files.

Supplemental Figure S1. Physical interactions between SWC4, YAF9A and SWC6.
Supplemental Figure S2. Arabidopsis SWC4 is nuclear localized, widely expressed and conserved in fungi, animals and plants.
Supplemental Figure S3. The *swc4*-1 mutation does not affect pollen viability**.**
Supplemental Figure S4. RNAi-mediated knockdown of *SWC4* expression in Col plants.
Supplemental Figure S5. SWC4 overexpression does not cause developmental alterations.
Supplemental Figure S6. Role of SWC4 on primary root elongation.
Supplemental Figure S7. Singular Enrichment Analysis (SEA) of Gene Ontology (GO) terms of misregulated genes in *swc4i* mutant.
Supplemental Figure S8. Comparisons of upregulated genes in *swr1*-c mutants.
Supplemental Figure S9. Comparisons of downregulated genes in *swr1*-c mutants.
Supplemental Figure S10. Specificity of α-HTA9 antibody.
Supplemental Figure S11. Representative genomic landscapes of H2A.Z (HTA9), H3 and Input ChIP-seq samples in two independent biological replicates (Rep).
Supplemental Figure S12. Metagenomic plots (showing only Chromosome 1) of HTA9 ChIP-seq signal across genes (A, C, E and G) and transposable elements (B, D, F and H) in WT replicate 1 (A,B) and replicate 2 (C,D) samples, and swc4i replicate 1 (E,F) and replicate 2 (G,H) samples.
Supplemental Figure S13. Metagenomic plots (showing only Chromosome 1) of H3 ChIP-seq signal across genes A, C, E and G) and transposable elements (B, D, F and H) in WT replicate 1 (A,B) and replicate 2 (C,D) samples, and swc4i replicate 1 (E,F) and replicate 2 (G,H) samples.
Supplemental Figure S14. Singular Enrichment Analysis (SEA) of Gene Ontology (GO) terms of genes with reduced HTA9 levels in *swc4i* mutant.
Supplemental Figure S15. Arabidopsis SWC4 protein bears a SANT/Myb_DMAP1 domain.
Supplemental Figure S16. SWC4 binds AT-rich DNA elements *in vitro*.
Supplemental Figure S17. Enrichment of SWC4 AT-rich DNA binding elements in the TSS regions of misregulated genes in *h2a*.z triple and *arp6*-10 mutants.
Supplemental Figure S18. *swc4i* plants show reduced levels of H2A.Z at *FT* chromatin**.**
Supplemental Figure S19. SWC4 is not required for H2A.Z deposition neither for the maintenance of H4K5 Ac levels at *FLC* chromatin**.**
Supplemental Figure S20. Specificity of the α-SWC4 antibody**.**
Supplemental Figure S21. SWC4 is required for ARP6 targeting at *FT* chromatin**.**

Supplemental Table 1. Oligonucleotide sequences used in this study.
Supplemental Table 2. Summary of RNA-seq experiments.
Supplemental Table 3. Summary of ChIP-seq experiments.

Supplemental Methods.

Supplemental Data Set Legends.
Supplemental Data Set1. Arabidopsis SWC6 interactors.
Supplemental Data Set2. RNA-seq data.
Supplemental Data Set3. HTA9 ChIP-seq data.
Supplemental Data Set4. Overlap between RNAseq and ChIP-seq data.
Supplemental Data Set5. Depicted location of PCR amplicons of SWC4 ChIP binding sites and the AT-rich motifs recognized by SWC4 in *FT*, *FUL*, *IAA19* and *ERF9* genomic regions.

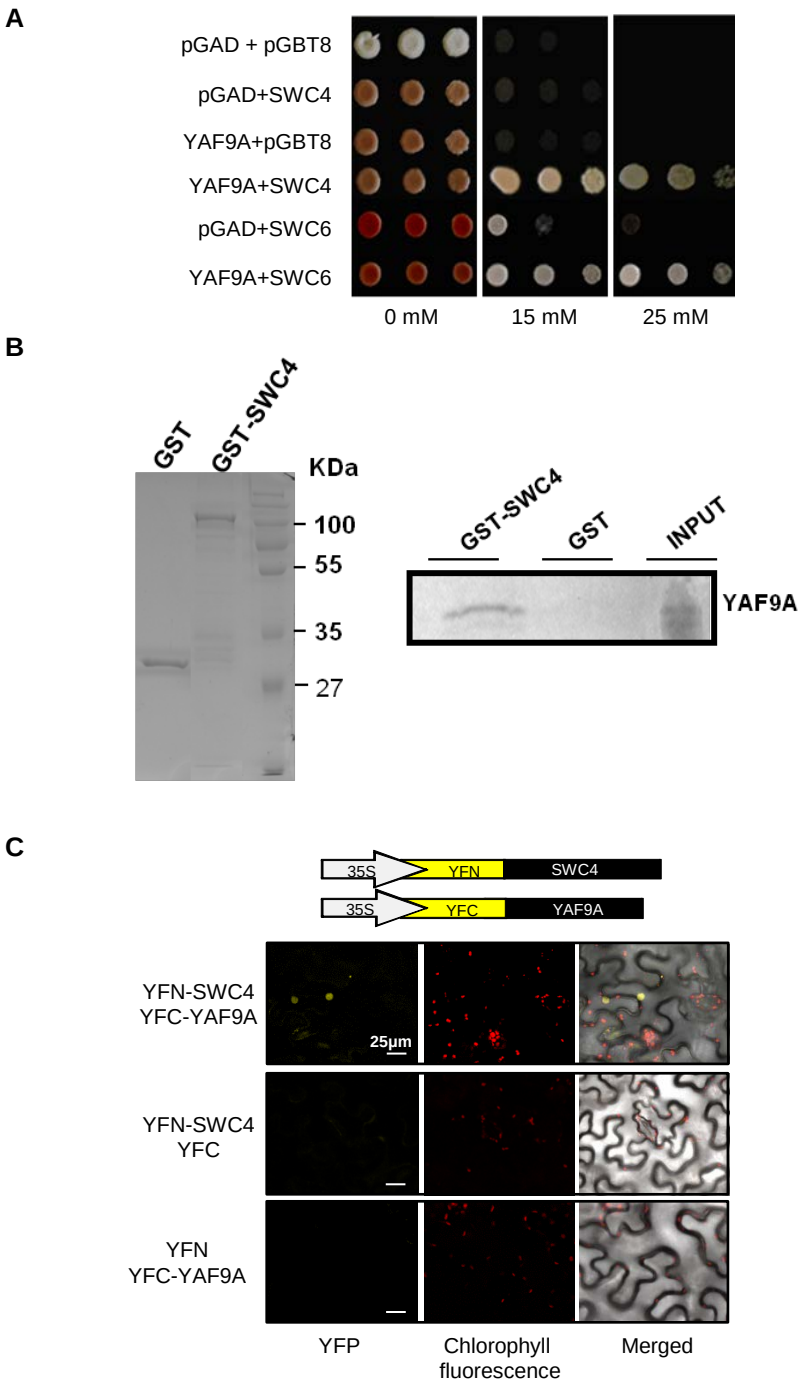

Supplemental Figure S1. Physical interactions between SWC4, YAF9A and SWC6.
(A) Y2H assays showing that YAF9 interacts with SWC4 and SWC6. Full-length SWC4 and SWC6 proteins were fused to the GAL4 DNA-binding domain, and YAF9A protein was fused to the GAL4 activation domain. Yeast transformed with these constructs or the corresponding empty vectors were grown with increasing concentrations of 3-AT. Three-fold decreasing dilutions of yeast were plated left to right in each panel.
(B) SWC4 interacts with YAF9A in vitro. Coomassie blue-stained SDS-PAGE showing GST and GST-SWC4 fusion protein expressed in E. coli BL21 Rosetta strain and purified with glutathione sepharose beads is shown on the left panel. The right panel show the result of a pull-down assay with GST and GST-SWC4 proteins incubated with [35S]Met-labeled YAF9A protein . Retained YAF9A protein was visualized after autoradiography of the dried gel.
(C) SWC4 interacts with YAF9A in planta. BiFC assays in *N. benthamiana* leaves co-expressing the N-terminus of YFP fused to SWC4 (YFN-SWC4) and the C- terminus of YFP to YAF9A (YFC-YAF9A) constructs. Yellow fluorescence in the nucleus indicates interaction. Negative controls included in the assay are shown.

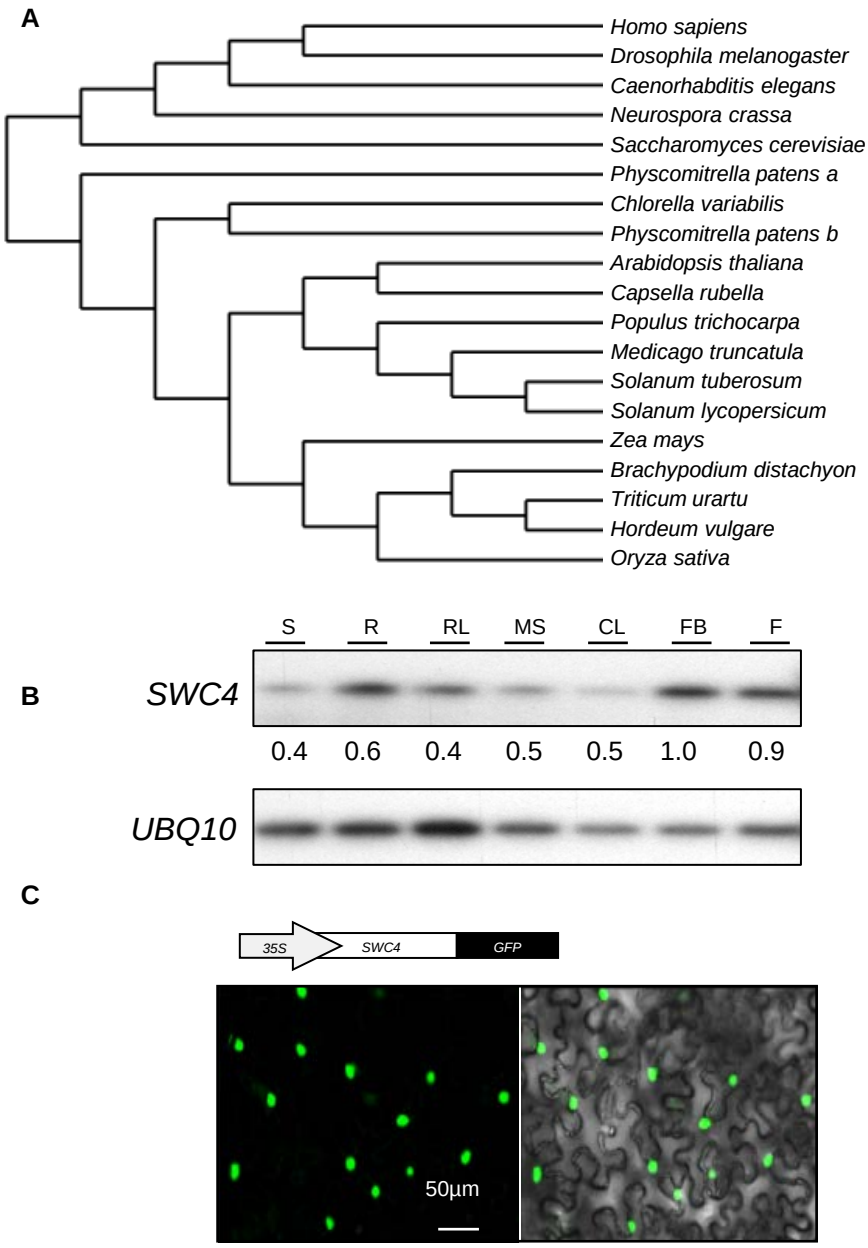

Supplemental Figure S2. *Arabidopsis* SWC4 is nuclear localized, widely expressed and conserved in fungi, animals and plants.

(A) Neighbour-joining protein sequence phylogeny showing SWC4/DMAP1 proteins from fungi, algae, plants and metazoans. The analysis was performed on the Phylogeny.fr web platform and comprised the following steps: sequences were aligned with MUSCLE, after alignment, ambiguous regions were removed with Gblocks, the phylogenetic tree was reconstructed using the maximum likelihood method implemented in the PhyML program, and graphical representation was performed with TreeDyn program.

(B) *SWC4* expression in different organs determined by quantitative RT-PCR and normalized against *UBQ10* expression (S, seedling; R, Roots; RL, rosette leaves; MS, main stem; CL cauline leaves; FB, flower buds; F, flowers).

(C) Transient expression of p35S:SWC4-GFP in *N. benthamiana*. Image of subcellular localization of SWC4-GFP protein in the nucleus of epidermal cells. Merge of fluorescence (green channel) and optical images (right panel) is shown.

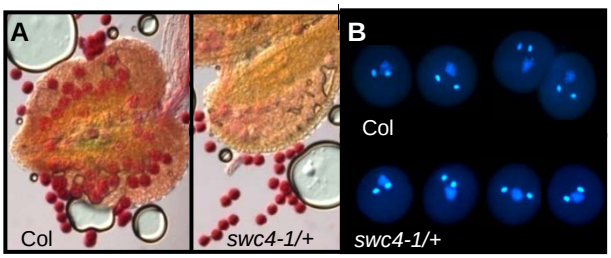

Supplemental Figure S3. The *swc4-1* mutation does not affect pollen viability.
(A) Detail of pollen from WT (left) and the *swc4-1*/+ mutant (right). Pollen grains (n=50) were isolated from the anthers of opened flowers and examined by Alexander staining. Viable pollen grains were stained as purple and dead pollen grains are dark green.
(B) DAPI staining of WT (upper panel) and *swc4-1*/+ mutant (lower panel) nuclei of pollen grains.

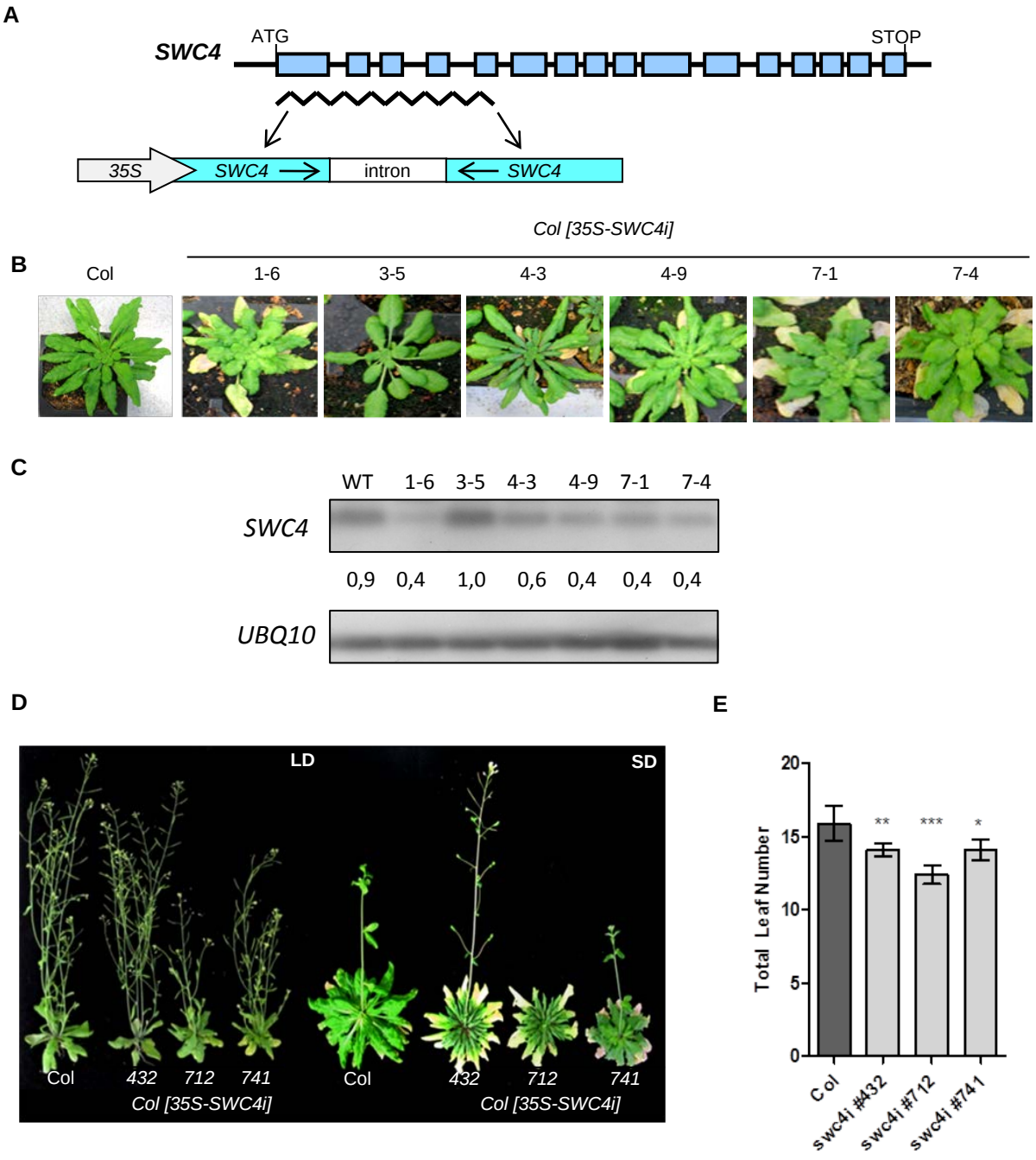

Supplemental Figure S4. RNAi-mediated knockdown of *SWC4* expression in Col plants.
(A) Schematic representation of the transformed *SWC4* RNAi construct containing an inverted repeat of 500 bp from the *SWC4* gene separated by an intron.
(B) Several T2 transgenic lines with a single insertion of the *SWC4* RNAi transgene grown in SD conditions.
(C) Quantitative RT-PCR analysis of relative *SWC4* transcript expression. RNA was extracted from Col and *SWC4* RNAi T2 seedlings (1-6, 3-5, 4-3, 4-9, 7-1, and 7-4 lines). There is specific reduction in the *SWC4* transcript levels in the different T2 *swc4i* transgenic plants analyzed compared with Col. *UBQ10* transcript was used as a loading control.
(D) Independent homozygous *SWC4i* T3 lines carrying only one transgene copy (432, 712, 741), grown during 4 weeks in LD and 13 weeks under SD conditions.
(E) Flowering time data of representative *SWC4i* knockdown lines under LD conditions (n= 15; error bars indicate ±sd.) (* p<0.05; ** p<0.01; *** p<0.001; Student´s t-test)

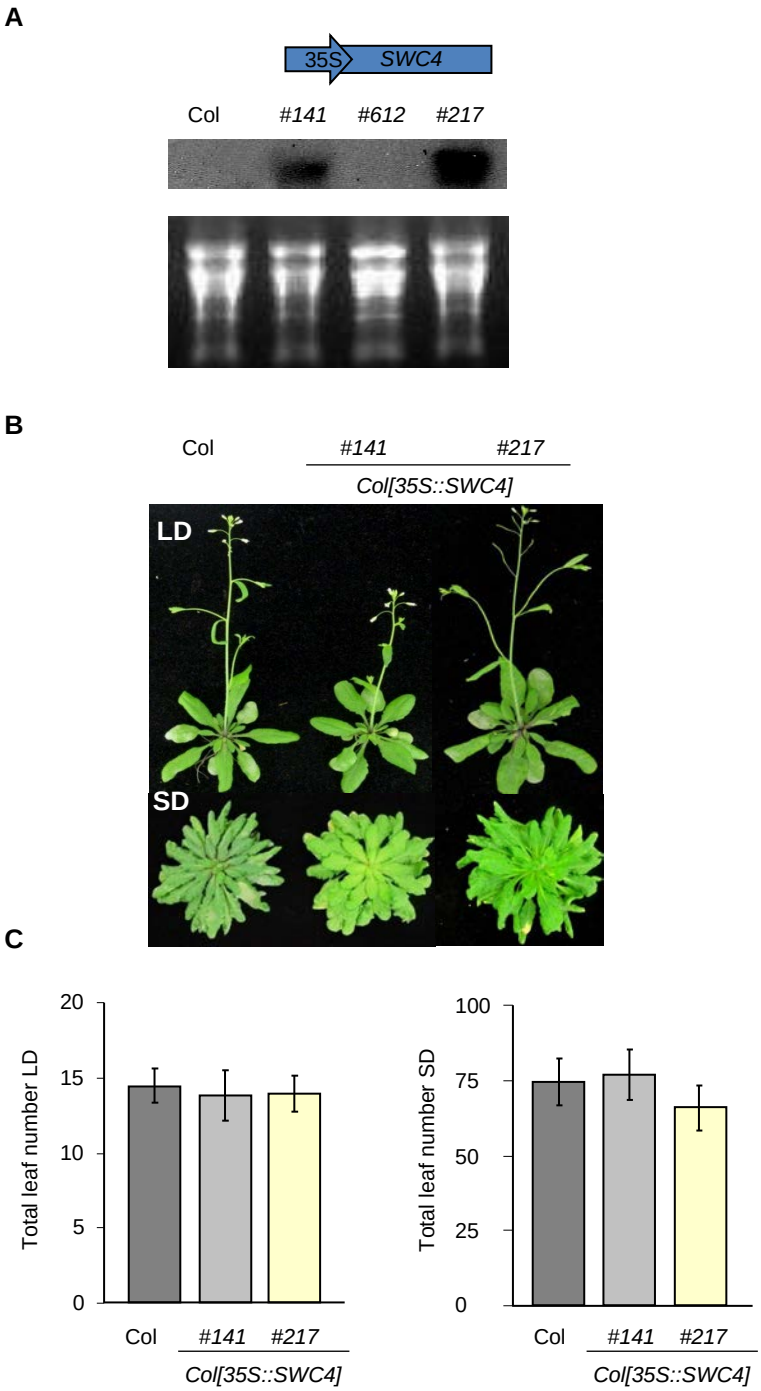

Supplemental Figure S5. *SWC4* overexpression does not cause developmental alterations.
(A) Overexpression of *SWC4* in Col background. Northern blots showing the levels of *SWC4* mRNA expression in different transgenic plants harbouring the *35S::SWC4* construct. Note that line 612 does not over-accumulate the transgene.
(B) Picture of representative transgenic lines (141 and 217) overexpressing *SWC4,* grown under LD conditions.
(C) Flowering time data of *SWC4* overexpressing lines under LD and SD conditions (n= 15; error bars indicate ±sd.)

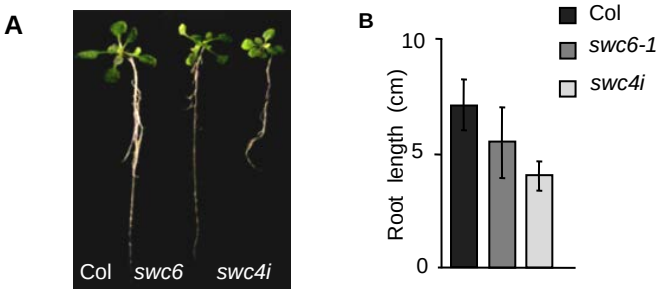

Supplemental Figure S6. Role of SWC4 on primary root elongation.
(A) Pictures of Col, *swc6-1* and *swc4i* seedlings grown vertically for 15 days on plates under *in vitro* culture conditions.
(B) Quantification of primary root length of 15 day-old Col, *swc6-1* and *swc4i* plantlets grown on vertical plates.

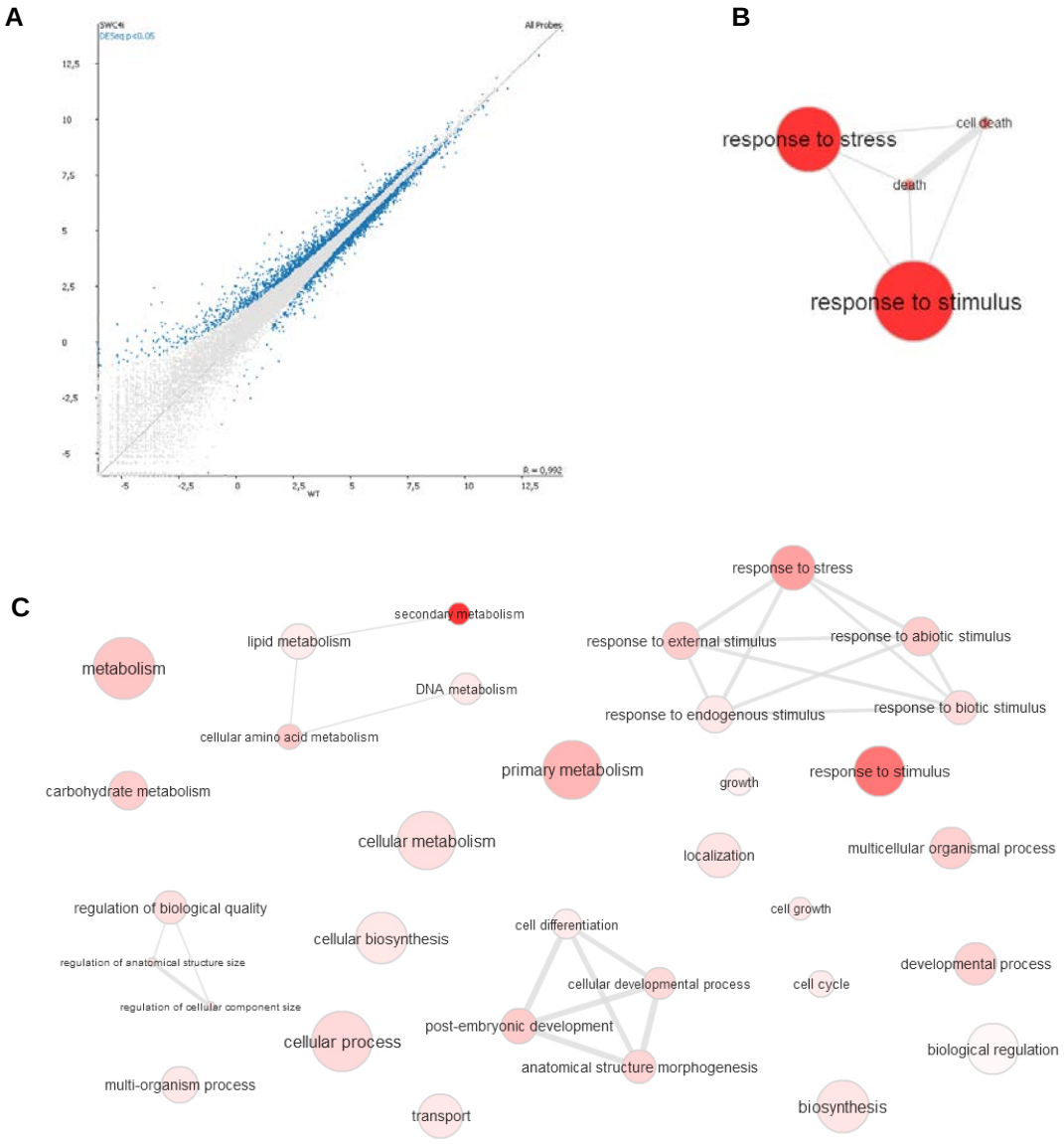

Supplemental Figure S7. Singular Enrichment Analysis (SEA) of Gene Ontology (GO) terms of misregulated genes in *swc4i* mutant.
(A) Scatter plot representation of log2 transformed Seqmonk RNA-seq quantification pipeline data. Probes defined by DESeq2 as differentially expressed genes are highlighted in blue.
(B, C) SEA of GO terms in "biological process" category from *swc4i* upregulated **(B)** and downregulated **(C)** genes lists. Analysis performed using AgriGO (Fisher test statistical analysis, $p<0.05$). Visualization with REVIGO ''Interactive graph'' view (allowed similarity =0.7). Bubble color indicates the user-provided p-value; bubble size indicates the frequency of the GO term in the underlying database. Highly similar GO terms are linked by edges in the graph, where the line width indicates the degree of similarity.

A

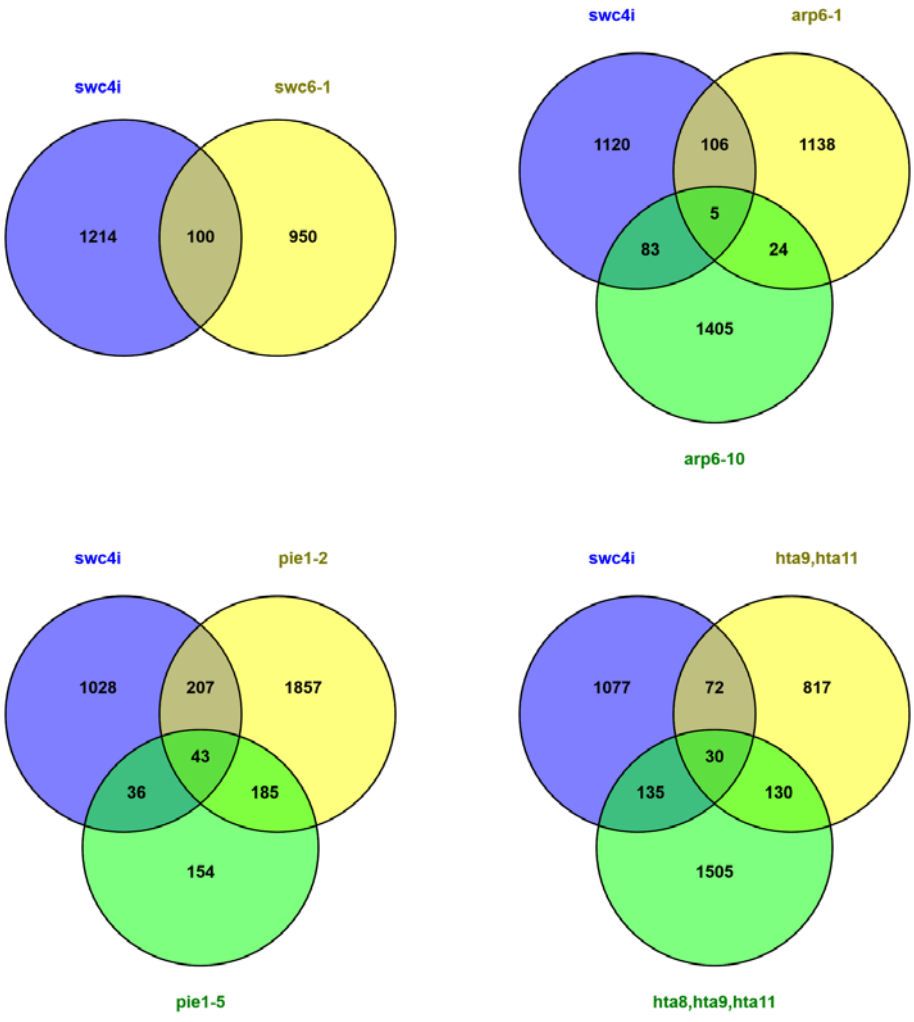

B

swc4i vs	p-value	score
swc6-1	1,2E-14	***
apr6-1	2,9E-12	***
arp6-10	9,9E-01	ns
pie1-2	1,3E-48	***
pie1-5	2,4E-39	***
hta9,hta11	1,7E-15	***
hta8,hta9,hta11	2,3E-25	***

Supplemental Figure S8. Comparisons of upregulated genes in *swr1-c* mutants
(A) Venn diagrams showing the overlap of upregulated genes between *swc4i* and other representative *swr1-c* mutants or plants depleted in H2A.Z. RNA seq analysis and published transcriptomic data (log2FC≥0.5) from *arp6-10* (Kumar and Wigge, 2010), *pie1-5* (March-Diaz et al., 2008), *hta8,9,11* triple mutant (Coleman-Derr and Zilberman, 2012a) and *swc6-1*, *arp6-1*, *pie1-2* and *hta9,hta11* mutants (Berriri et al., 2016).
(B) Statistical significance of the overlap with *swc4i* misregulated genes was determined performing a hypergeometric test (ns, not significant; ****P*≤0.001).

A

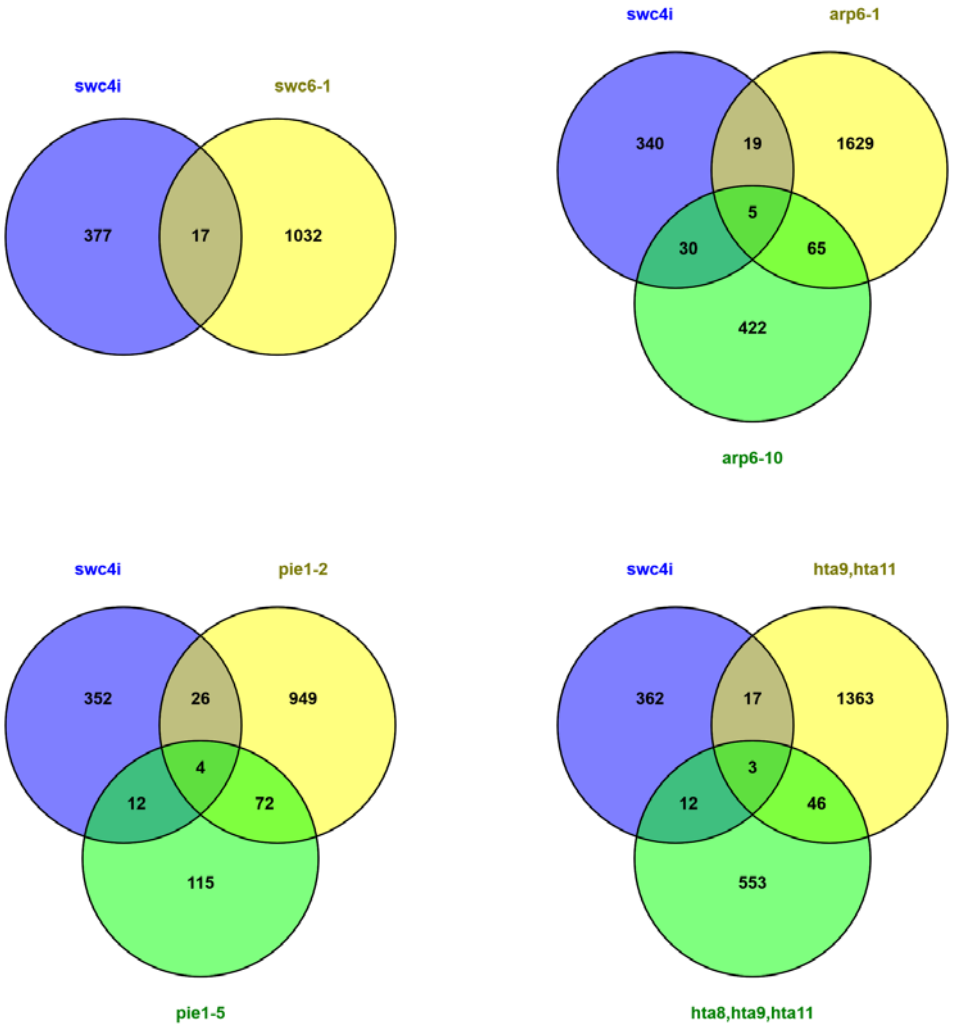

B

swc4i vs	p-value	score
swc6-1	1,4E-01	ns
apr6-1	2,7E-01	ns
arp6-10	7,5E-18	***
pie1-2	1,8E-05	***
pie1-5	6,1E-09	***
hta9,hta11	2,0E-01	ns
hta8,hta9,hta11	9,2E-03	***

Supplemental Figure S9. Comparisons of downregulated genes in *swr1-c* mutants
(A) Venn diagrams showing the overlap of downregulated genes between *swc4i* and other representative *swr1-c* mutants or plants depleted in H2A.Z. RNA seq analysis and published transcriptomic data (log2FC≤0.5) from *arp6-10* (Kumar and Wigge, 2010), *pie1-5* (March-Diaz et al., 2008), *hta8,9,11* triple mutant (Coleman-Derr and Zilberman, 2012a) and *swc6-1*, *arp6-1*, *pie1-2* and *hta9,hta11* mutants (Berriri et al., 2016).
(B) Statistical significance of the overlap with *swc4i* misregulated genes was determined performing a hypergeometric test (ns, not significant; ****P*≤0.001).

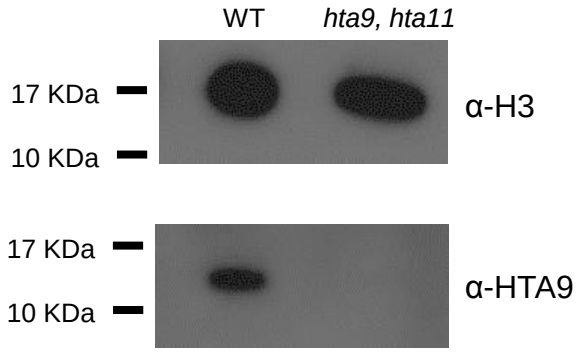

Supplemental Figure S10. Specificity of α-HTA9 antibody
Histone protein extracts from *Arabidopsis* WT and *hta9 hta11* double mutant (March-Diaz et al., 2008) were tested by western blot against α-H3 (Abcam ab1791) and α-HTA9 antibody (Agrisera, AS10718). As shown we could not detect any band in *hta9 hta11* double mutant histone extracts.

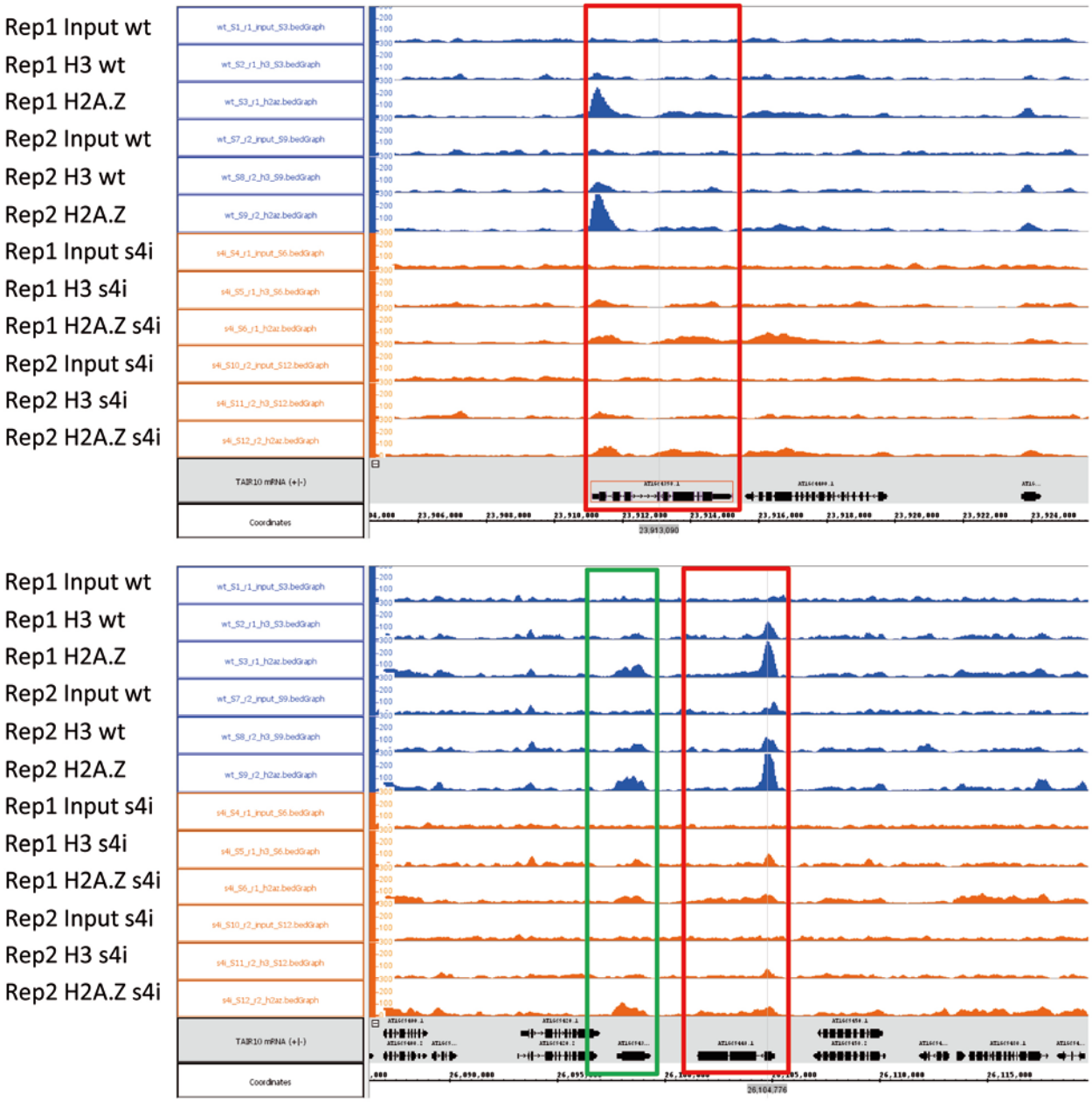

Supplemental Figure S11. Representative genomic landscapes of H2A.Z (HTA9), H3 and Input ChIP-seq samples in two independent biological replicates (Rep).
Red boxes highlights an example of a gene with reduced H2A.Z levels in *swc4i* samples, whereas the green box shows a gene region with no changes in H2A.Z distribution between WT and *swc4i*.

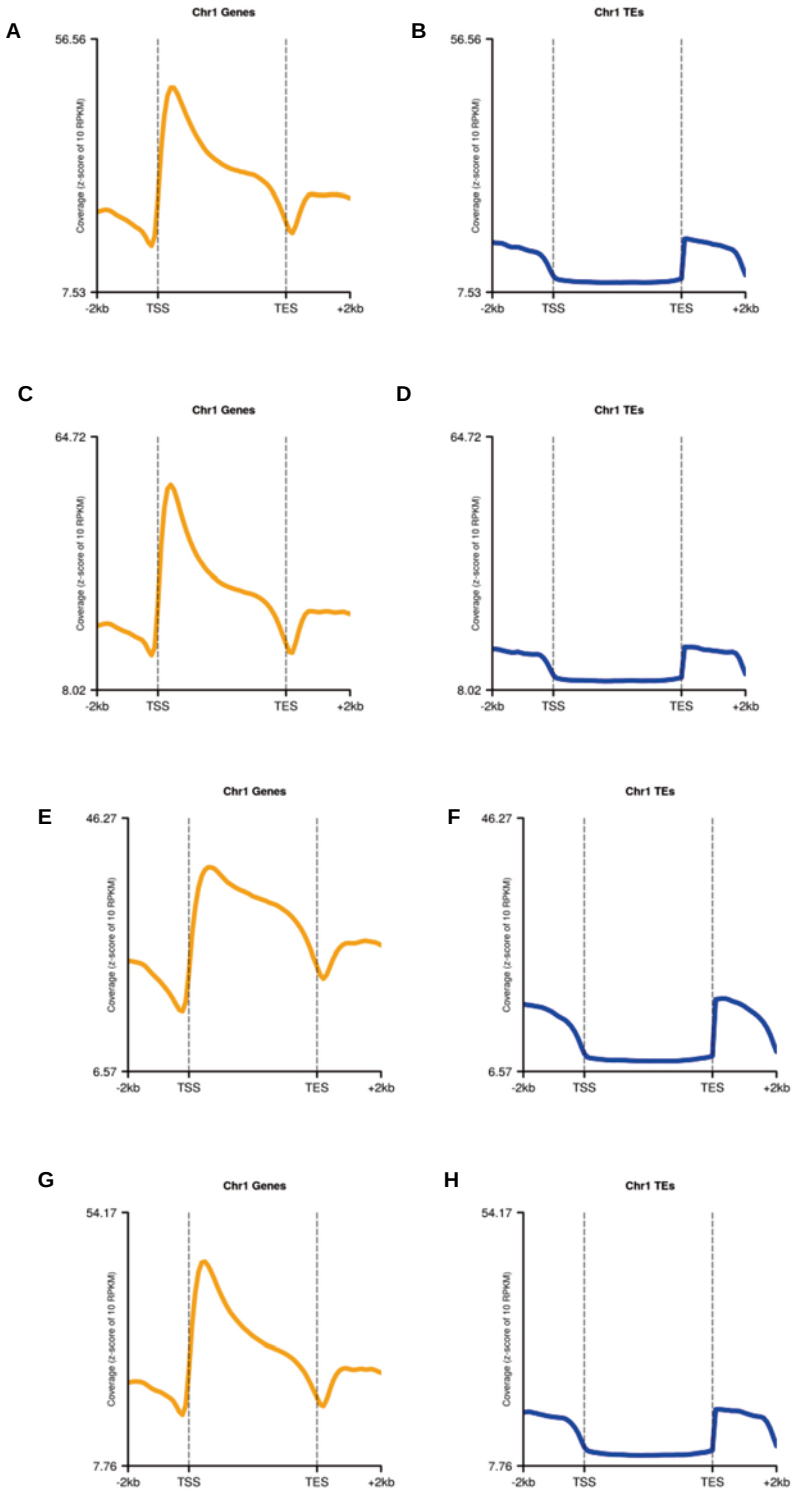

Supplemental Figure S12. Metagenomic plots (showing only Chromosome 1) of HTA9 ChIP-seq signal across genes (**A**, **C, E** and **G**) and transposable elements (**B**, **D**, **F** and **H**) in WT replicate 1 (**A**,**B**) and replicate 2 (**C**,**D**) samples, and *swc4i* replicate 1 (**E**,**F**) and replicate 2 (**G**,**H**) samples.

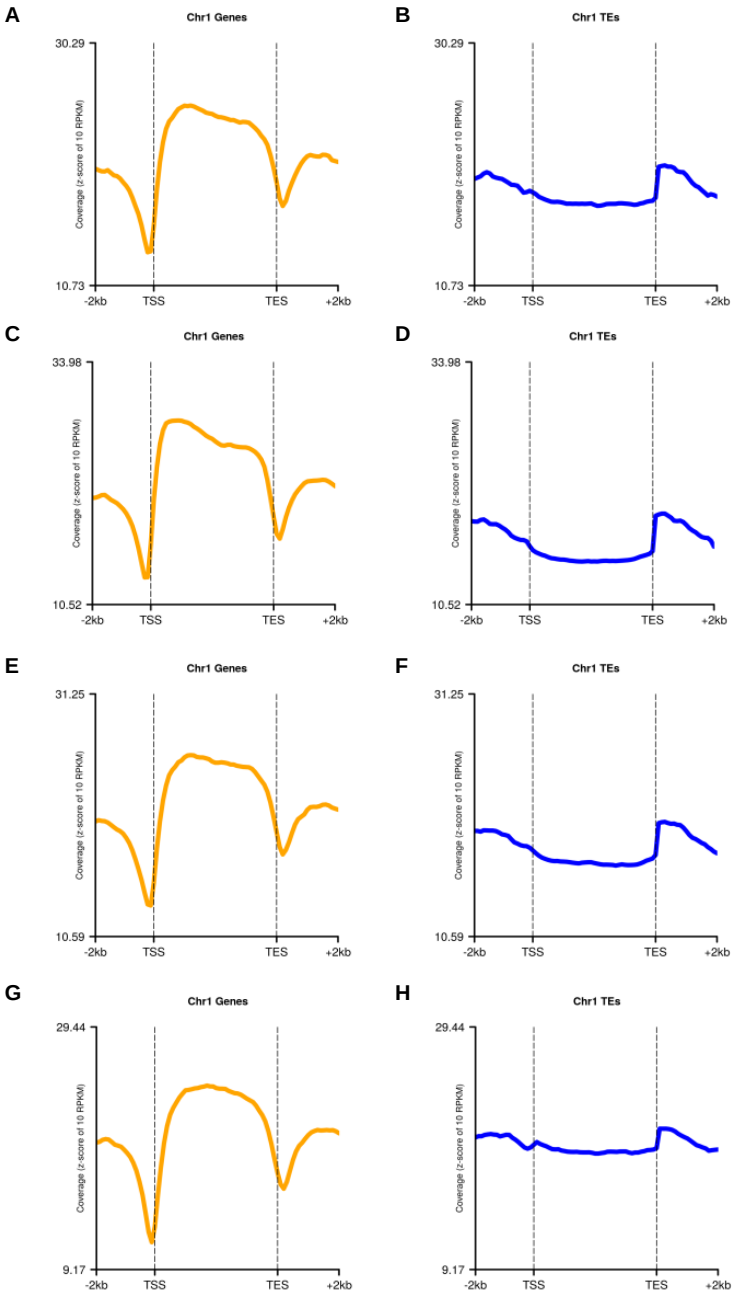

Supplemental Figure S13. Metagenomic plots (showing only Chromosome 1) of H3 ChIP-seq signal across genes **A**, **C, E** and **G**) and transposable elements (**B**, **D**, **F** and **H**) in WT replicate 1 (**A**,**B**) and replicate 2 (**C**,**D**) samples, and *swc4i* replicate 1 (**E**,**F**) and replicate 2 (**G**,**H**) samples.

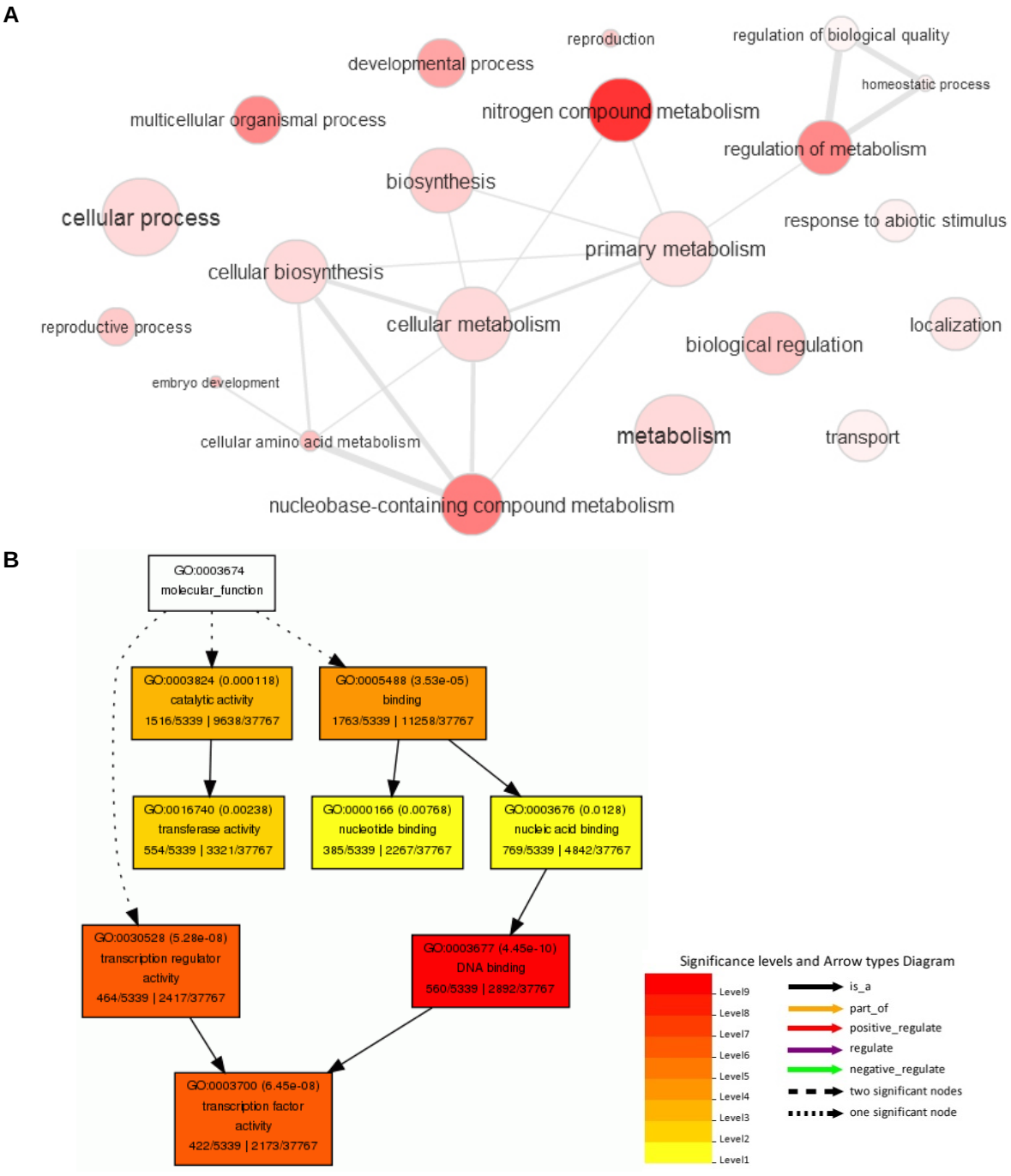

Supplemental Figure S14. Singular Enrichment Analysis (SEA) of Gene Ontology (GO) terms of genes with reduced HTA9 levels in *swc4i* mutant.
(A) SEA of GO terms in "biological process" category using AgriGO (Fisher test statistical analysis, $p<0.05$). Visualization with REVIGO ''Interactive graph'' view (allowed similarity =0.7). Bubble color indicates the user-provided p-value; bubble size indicates the frequency of the GO term in the underlying database. Highly similar GO terms are linked by edges in the graph, where the line width indicates the degree of similarity.
(B) Tree graph representation of over-represented GO terms in "molecular function" category obtained using AgriGO (Fisher test statistical analysis, $p<0.05$). Significant terms are marked with colour, non-significant ones are shown in white boxes. This hierarchical graph is represented ranked from top to bottom.

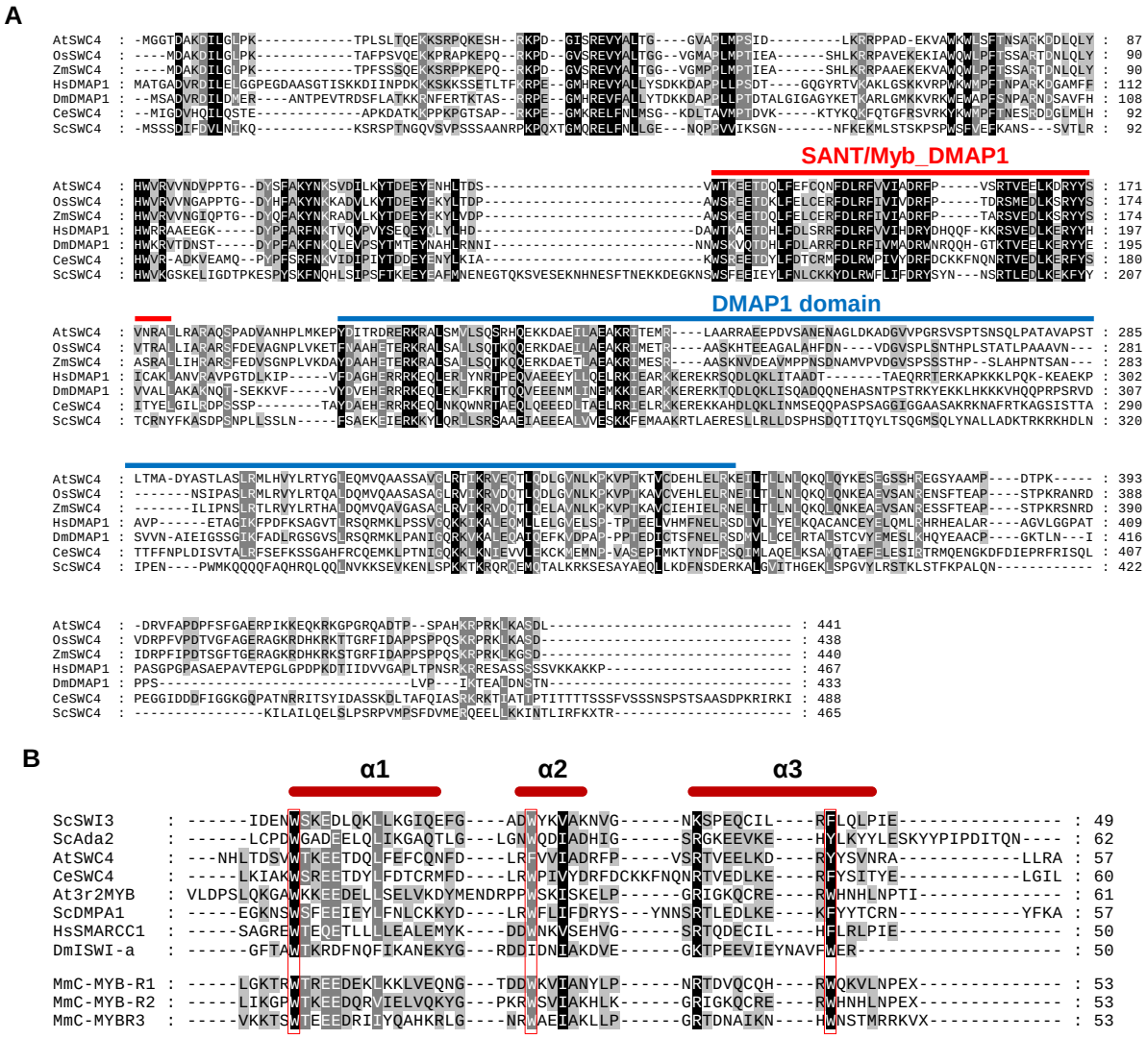

Supplemental Figure S15. *Arabidopsis* SWC4 protein bears a SANT/Myb_DMAP1 domain.
(A) Sequence comparisons of SWC4 protein from different organisms: At, *Arabidopsis thaliana*; Os, *Oryza sativa*; Zm, *Zea mays*; Hs, *Homo sapiens*; Dm, *Drosophila melanogaster*; Ce, *Caenorhabditis elegans*; Sc, *Saccharomyces cerevisiae*, using ClustalX v1.81. Red box line indicates the SANT/Myb_DMAP1 domain (IPR032563) whereas the blue line refers to the conserved DMAP1 C-terminal domain (IPR008468).
(B) SANT/Myb_DMAP1 domain shows strong similarity to the Myb DNA-binding domain. Sequence comparisons of SANT/Myb_DMAP1 domain from *Arabidopsis* SWC4 and At3r2MYB proteins; yeast SWI3, ADA2 and SWC4/DMAP1 proteins; *C. elegans* SWC4 protein; Human SMARCC1 protein and *D. melanogaster* ISWI protein, with Myb domain (repeats R1, R2 and R3) from mouse using ClustalX v1.81: Hs, *Homo sapiens*; Sc, *Saccharomyces cerevisiae*; At, *Arabidopsis thaliana*; Ce, *Caenorhabditis elegans*; Dm, *Drosophila melanogaster*; Mm, *Mus musculus*.
In both **(A)** and **(B)** panels the amino acid residues in black are identical or functionally similar in 100% of compared proteins. The amino acid residues in dark grey are identical or functionally similar in 80% whereas residues in soft grey indicate identity in 40% of compared proteins. Red boxes highlight the bulky hydrophobic residues that are predicted to form the hydrophobic core of the SANT/Myb domain.

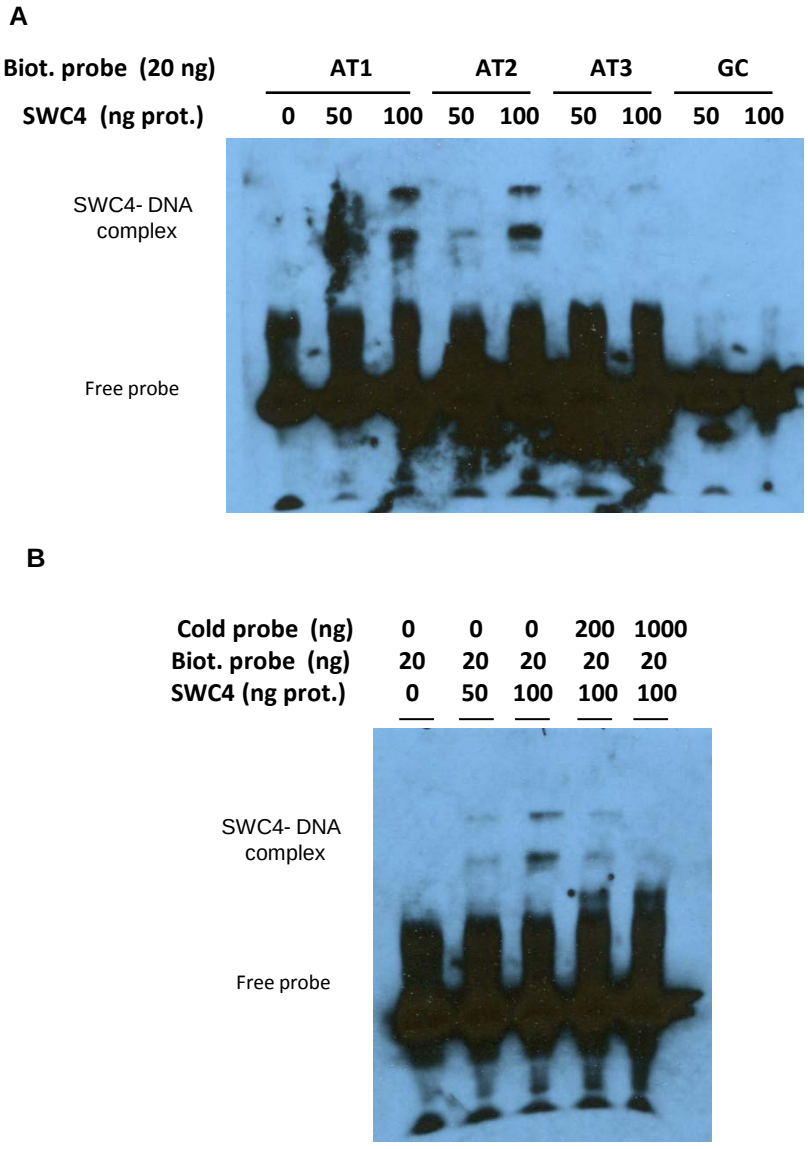

Supplemental Figure S16. SWC4 binds AT-rich DNA elements *in vitro*.
(A). Gel shift assay with SWC4 and three different AT-rich probes: AT1 (AATTAAAT), AT2 (AAATAAAA) and AT3 (TTAATTAA), ranked among the top 8-mer motifs identified in PBM assay; or one 'GC'-rich (AGCCCCCG) probe. Binding reactions were performed by incubating 20 ng of double stranded biotinylated probes with 50 or 100 ng of purified SCW4-MBP for 45 min at 4ºC, and were later resolved in 5% PAGE and transferred to membrane. Biotin was detected with LightShift Chemiluminescent EMSA kit . SWC4 DNA complexes were revealed with the AT-rich probes but not with the GC-rich probe.
(B) SWC4 binds specifically to AT-rich probes. Binding specificity of SWC4 to AT1 probe was tested by adding 10 and 50 times more unlabeled competitor probe than biotinilated probe in the binding reactions.

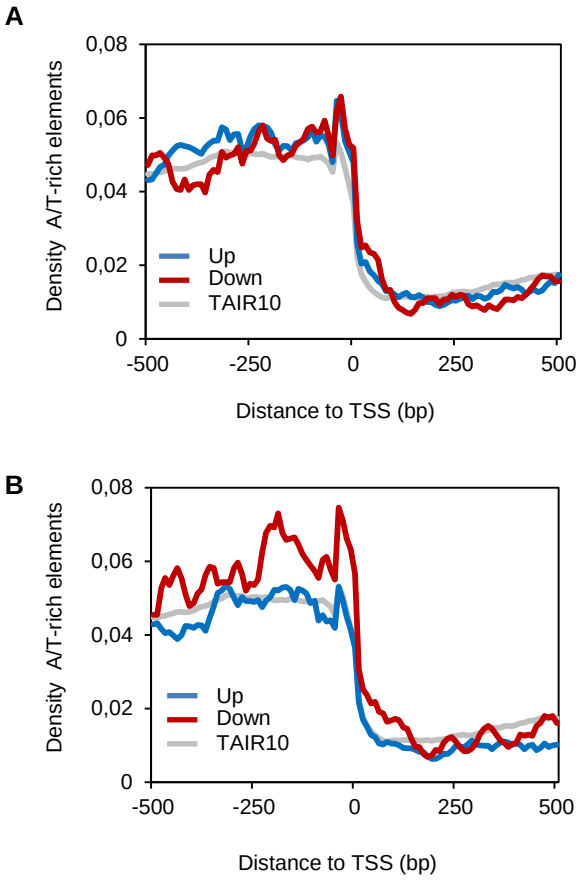

Supplemental Figure S17 Enrichment of SWC4 AT-rich DNA binding elements in the TSS regions of misregulated genes in *h2a.z* triple and *arp6-10* mutants.
Plots represents the density of SWC4 AT-rich elements around the TSS (position 0, x-axis), covering 0.5 kb upstream and downstream of the TSS, and include average densities for *Arabidopsis* genes (TAIR10, grey line), genes up-regulated (Up, blue line) and down-regulated (Down, red line) in the *h2a.z* triple (Coleman-Derr and Zilberman, 2012b) **(A)** and *arp6-10* (Kumar and Wigge, 2010) **(B)** mutants.

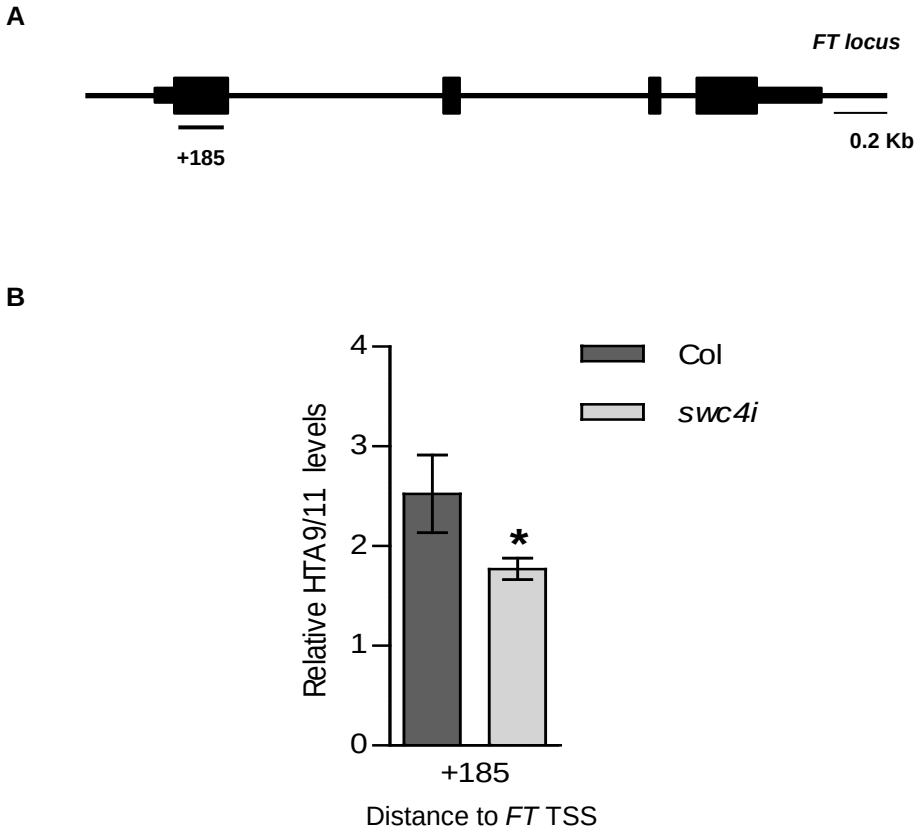

Supplemental Figure S18. *swc4i* plants show reduced levels of H2A.Z at *FT* chromatin.
(A) Schematic representation of *FT* locus indicating the region analyzed by ChIP.
(B) ChIP experiment using α-HTA9/11 antibody (Zhang et al., 2015) in 9 day-old WT and *swc4i* seedlings. Data are represented as the fraction of immunoprecipitated DNA normalized to *ACT* and is the average of four Q-PCR reactions from two biological replicates. Error bars indicate ± sd (* p<0.05; Student´s t-test).

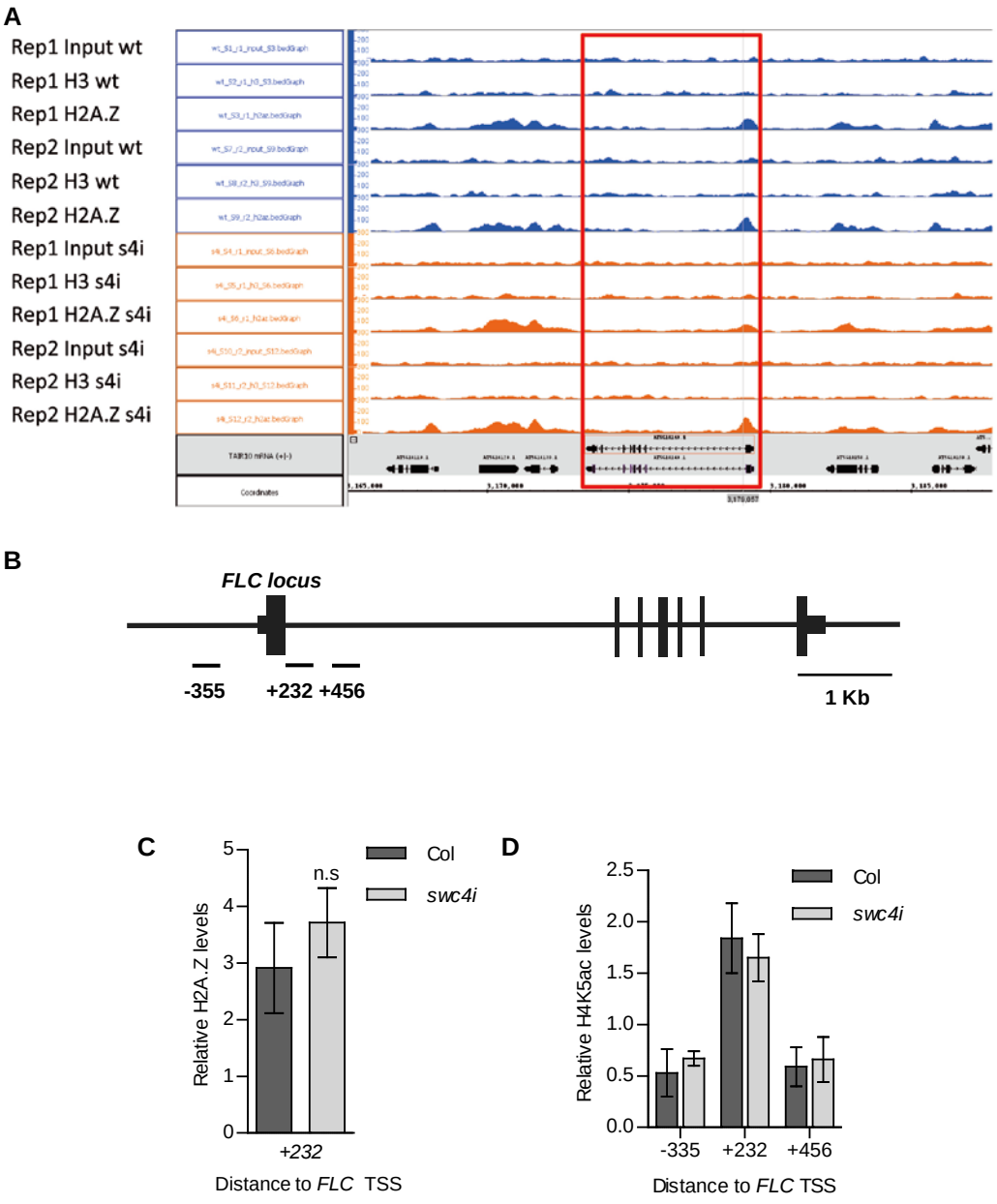

Supplemental Figure S19. SWC4 is not required for H2A.Z deposition neither for the maintenance of H4K5 Ac levels at *FLC* chromatin.
(A) Genomic landscapes of H2A.Z (HTA9), H3 and Input ChIP-seq samples in the genomic region of *FLC* locus. No changes in H2A.Z distribution in *FLC* chromatin between WT and *swc4i* (red box) were detected in our ChIP-seq experiments using SICER (Supplemental Data S3).
(B) Schematic representation of *FLC* locus indicating the regions analyzed by ChIP.
(C-D) ChIP experiments using α-HTA9/11 **(C)** and α-H4K5ac **(D)** in 10 day-old WT and *swc4i* seedlings**.** *swc4i* plants do not show changes in the levels of H2A.Z neither in H4K5ac at *FLC* chromatin. Data are represented as the fraction of immunoprecipitated DNA normalized to *ACT* and is the average of 4 Q-PCR reactions from 2 biological replicates. Error bars indicate ±sd; n.s. is not statistically significant; Student´s t-test.

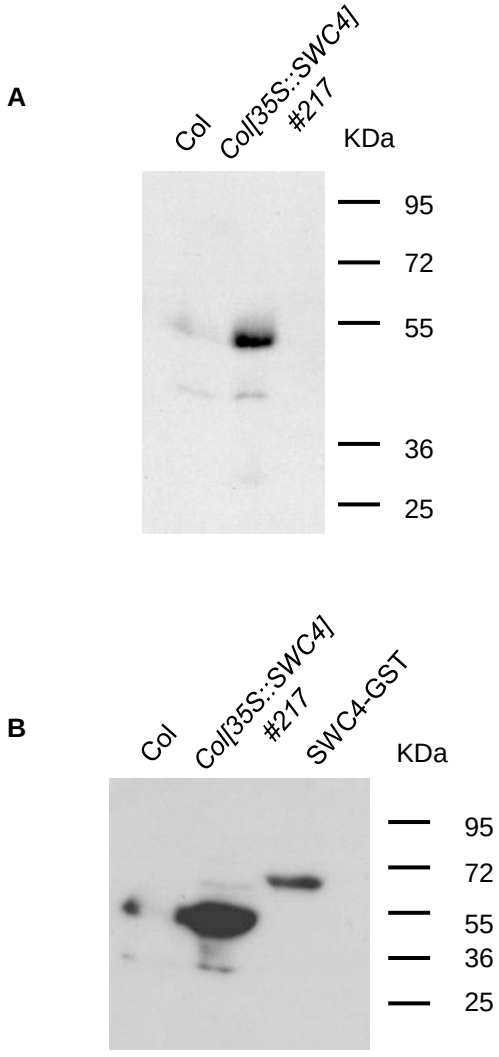

Supplemental Figure S20. Specificity of the α-SWC4 antibody.
Western blots using total protein extracts from *Arabidopsis* WT and SWC4 overexpressor line (p*35S:SWC4#217*) seedlings **(A, B)** and recombinant SWC4-GST protein purified from *E.coli* **(B)**.

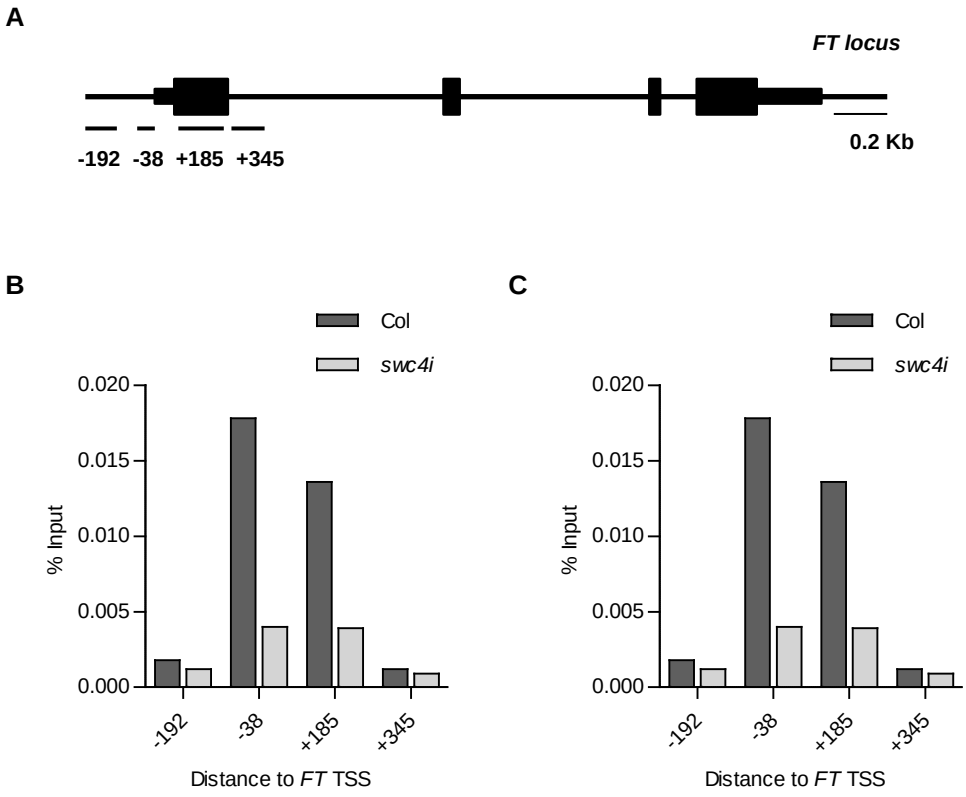

Supplemental Figure S21. SWC4 is required for ARP6 targeting at *FT* chromatin.
(A) Schematic representation of *FT* locus indicating the regions analyzed by ChIP.
(B-C) *swc4i* plants show reduced levels of ARP6 binding at *FT* chromatin. Two independent ChIP experiments using α-ARP6 antibody (Zhao et al., 2018) in WT and *swc4i* seedlings are shown. in the figure. Data are the average of technical triplicates Q-PCR reactions and represent the fraction of immunoprecipitated DNA normalized to the DNA concentration measured by Qubit assay.

Supplemental Table 1. Oligonucleotide sequences used in this study:

FORWARD	REVERSE	Used for
TTAGCTCTAACGAATCGAACCAAT	GGACAGCAAAAGTTACTCAATGACA	Genotyping of *swc4-1* allele
CTGAAATTCTCTTCCTTGTCACG	TTCTTCATTGAGAGAGAGTGAGAAA	SWC4 genomic complementation
ATGGGCGGTACGGACGCGAAGGACA	CCTCCACAGTCCGTGATACTGGAAA	Quantitative RT-PCR expression analysis of *SWC4*
GATCTTTGCCGGAAAACAATTGGAGGATGGT	CGACTTGTCATTAGAAAGAAAGAGATAACACG	Quantitative RT-PCR expression analysis of *UBQ10*
TGTCGCCATCCAAGCTGTTCTCT	GTGAGACACCATCACCAGAAT	Q-PCR expression of *ACT1*
CAGCAGATGTTGCAAACCATCCTCT	GGGTAGAGGCATAATCTGCCATAGT	Q-PCR expression analysis of *SWC4*
CCGAACTCATGTTGAAGCTTGTTGAG	CGGAGATTTGTCCAGCAGGTG	Q-PCR expression analysis of *FLC*
GCCTTTGAGCTCTCAGTGCTTTG	CTTCGCTTTCATGAGATCCCCAC	Q-PCR expression analysis of *SOC1*
CTTGGCAGGCAAACAGTGTATGCAC	GCCACTCTCCCTCTGACAATTGTAGA	Q-PCR expression analysis of *FT*
CTGCGACTCAGGGAATCTTCTAA	TTGTGCCATTGAATTGAACCC	Q-PCR expression analysis of *UBC*
GTGGCTACCAAGTGGGAGAT	ACACATTGTCGTCTTATTTCA	ChIP -192 *FT* region
TGATTTCACCGACCCGAGTT	AGGCATGAACCCTCTACACATATTTA	ChIP -38 *FT* region
GAGACCCTCTTATAGTAAGCAGAGTT	CCTGAGGTCTTCTCCACCA	ChIP +185 *FT* region
GTTCTTTCACTTGAACTCCCTTTTG	CCCAAGAAATATTTTCAGTATACCCC	ChIP +345 *FT* region
TGTCGCCATCCAAGCTGTTCTCT	GTGAGACACCATCACCAGAAT	ChIP ACT2
CGCATCCTCAGTTGACCTGTC	TTGTAGTAATGGCACCGCGTC	ChIP IAA19
AGGCGAACGGTAGAAGCATTG	AGCCAAACCCGGGTTTTCTTT	ChIP ERF9
GGGAAGAGGTAGGGTTCAGCT	GACGATGAGAGCAACCTCAGC	ChIP FUL
TAGGGTTCTTAGTTGATCTTGTATTGAGCTC	TTTGCTCTCAAACTCTCAATTGAAGTTT	ChIP Ta3

Supplemental Table 2. Summary of RNA-seq experiments

Sample[1]	Total reads[2]	Mapped reads[3]
Col R1	44 753 280	98.2%
Col R2	45 033 728	98.2%
swc4i R1	44 776 066	98.1%
swc4i R2	45 031 418	98.2%

[1] Biological replicates
[2] Clean data reads
[3] TOPHAT overall read mapping rate

Supplemental Table 3. Summary of ChIP-seq experiments

Sample	Reads processed	Reads with single alignment (mapping efficiency)	Duplicated reads	Reads with multiple alignment	Reads with no alignment
Col R1 Input	12 972 396	5 011 877 (38.6%)	1 486 237	5 863 889 (45.20%)	2 096 630 (16.16%)
Col R1 H3	12 433 974	2 679 627 (21.6%)	231 660	8 278 624 (66.58%)	1 475 723 (11.87%)
Col R1 HTA9	8 232 972	5 174 195 (62.9%)	648 209	1 866 133 (22.67%)	1 192 644 (14.49%)
Col R2 Input	15 024 363	5 215 991 (34.7%)	1 804 470	7 743 297 (51.54%)	2 065 075 (13.74%)
Col R2 H3	13 054 599	5 220 453 (40.0%)	294 072	6 398 353 (49.01%)	1 435 793 (11.00%)
Col R2 HTA9	11 328 063	4 940 982 (43.6%)	1 471 798	4 342 471 (38.33%)	2 044 610 (18.05%)
swc4i R1 Input	15 505 703	6 088 090 (39.3%)	2 107 815	6 897 406 (44.48%)	2 520 207 (16.25%)
swc4i R1 H3	12 606 116	3 118 173 (24.7%)	273 403	7 799 465 (61.87%)	1 688 478 (13.39%)
swc4i R1 HTA9	10 741 435	6 714 797 (62.5%)	1 720 953	2 270 041 (21.13%)	1 756 597 (16.35%)
swc4i R2 Input	15 139 729	5 284 312 (34.9%)	1 364 250	7 365 656 (48.65%)	2 489 761 (16.45%)
swc4i R2 H3	15 338 608	4 314 047 (28.1%)	290 274	9 640 286 (62.85%)	1 384 275 (9.02%)
swc4i R2 HTA9	13 409 878	5 295 375 (39.5%)	1 108 660	5 756 885 (42.93%)	2 357 618 (17.58%)

Supplemental Methods

Proteomics data analysis

For analysis of pull-down samples, proteins were digested using the in-gel digestion protocol as previously described (Bonzon-Kulichenko et al., 2011), with minor modifications. Briefly, proteins were extracted from beads by boiling in loading buffer containing Dithiothreitol (DTT), and the supernatants were run by conventional SDS-PAGE until the front entered 3 mm into the resolving gel. The protein band containing the whole proteome was visualized by Coomassie staining, excised, cut into cubes, subjected to reduction with 10 mM DTT and alkylation in 50 mM iodoacetamide, and digested overnight at 37º C with 60 ng/ml modified trypsin (Promega, Madison, WI, USA) at 12:1 protein:trypsin (w/w) ratio in 50 mM ammonium bicarbonate, pH 8.8 containing 10% acetonitrile. The resulting tryptic peptides were extracted by incubation in 12 mM ammonium bicarbonate pH 8.8 and later, 0.5% Trifluoroacetic acid (TFA). TFA was added to a final concentration of 1% and the peptides were finally desalted onto C18 Oasis-HLB cartridges and dried-down for further analysis.

For label-free analysis, digested peptides were loaded into the LC-MS/MS system for on-line desalting onto C18 cartridges and analyzed by LC-MS/MS using a C-18 reversed phase nano-column (75 µm I.D. x 25 cm, 2 µm particle size, Acclaim PepMap RSLC, 100 C18; Thermo Fisher Scientific, Waltham, MA, USA) in a continuous acetonitrile gradient consisting of 0-30% B in 120 min, 50-90% B in 3 min (A= 0.5% formic acid; B=90% acetonitrile, 0.5% formic acid). A flow rate of 200 nl/min was used to elute peptides from the RP nano-column to an emitter nanospray needle for real time ionization and peptide fragmentation on an Orbitrap Elite mass spectrometer (Thermo Fisher). An enhanced FT-resolution spectrum (resolution=70.000) followed by the CID MS/MS spectra from the 12 most intense parent ions were analyzed along the chromatographic run. Dynamic exclusion was set at 30 s.

For peptide identification, all spectra were analyzed with Proteome Discoverer (version 1.4.0.29, Thermo Fisher Scientific) using SEQUEST-HT engine (Thermo

Fisher Scientific). Database search was performed against Uniprot database containing all sequences from *Arabidopsis thaliana* and crap contaminants (February 28th, 2013; 31930 sequences), using the following parameters : trypsin digestion with 2 maximum missed cleavage sites, precursor and fragment mass tolerances of 600 ppm and 1.2 Da, respectively carbamidomethyl cysteine as fixed modification and methionine oxidation as dynamic modifications. Peptide identification was validated using the probability ratio method (Martinez-Bartolome et al., 2008) with an additional filtering for precursor mass tolerance of 12 ppm (Bonzon-Kulichenko et al., 2014). False discovery rate (FDR) was calculated using inverted databases and the refined method (Navarro et al., 2014) was used to filter peptides for quantitation, as previously described (Jorge et al., 2014). Proteins were quantified at each condition on the basis of the number of peptides identified at 1% FDR.

BiFC studies

SWC4 and YAF9A full length coding sequences were cloned in pYFN43 and pYFC43 vectors respectively to produce SWC4 fused to the N-terminal part of YFP (YFN-SWC4) and YAF9A fused to the C-terminal part of the YFP (YFC-YAF9A). BiFC experiments were performed as described (Lazaro et al., 2012). Fluorescent interactions were visualized under a Leica TCS SP2 confocal microscope set at 552–560 nm. Images were analyzed employing Leica LCSLite software.

In Vitro Pull-Down Assays

The GST and GST-SWC4 constructs in pGEX2TK vectors were expressed in *Escherichia coli* BL21 Rosetta strain and the proteins GSTor GST-SWC4 were purified with glutathione sepharose 4B beads (GE Amersham). In vitro transcription/ translation YAF9A reactions were performed with the TNT Quick Coupled Transcription/Translation System (Promega) in the presence of [35S]Met (Amersham Biosciences). For pull-down assays, 500 ng of GST and GST-SWC4

bound to beads was incubated with 15 μL of the TNT reaction in 200 μL of binding buffer containing 20 mM Tris-HCl pH 7.0, 100 mM NaCl, 1 mM EDTA, 10% glicerol, and 0.01% Nonidet P-40. The mixture was incubated at room temperature for 1 h and then washed five times with washing buffer (binding buffer supplemented with 500 mM NaCl). Samples were boiled in the presence of Laemmli buffer and analyzed by SDS-PAGE, transferred to nylon membrane and followed by autoradiography.

Histone preparations and western blot assays

Histone preparation form α-HTA9 were obtained were obtained by nuclear protein acid extraction, followed by acetone precipitation and resuspended in urea. SDS-PAGE and Western blot analyses were performed according to standard procedures using BSA as blocking agent.

Preparation of SWC4 antigen

The plasmid pGEX-2t/SWC4 was obtained from pGEX-2tK expression vector (INVITROGEN) by standard PCR techniques and was transformed into *E. coli* BL21 Rossetta cells. GST fusion protein was grown from 0.4mM Isopropyl β-D-1-thiogalactopyranoside (IPTG) induced bacterial cell cultures during 2 hours and purified using glutathione sepharose 4B beads (GE LifeSciences), according to standard protocols. Glutathione S-transferase (GST)-tag was removed with thrombin incubating 16 hours/ 37ºC ratio 1/100 and finally thrombin was inactivated with 0.3mM Phenylmethylsulfonyl Fluoride. GST-tag was retained with glutathione sepharose beads 2 hours longer, following steps for purification recommended by INVITROGEN. Recombinant proteins were eluted in 10 mM reduced glutathione 50 mM Tris-HCl, pH 8.0. The purity of the recombinant protein was estimated by SDS-PAGE techniques (≥90%), and the concentration was detected by the Bradford method. 0.5-1mg/ml of cleaved SWC4 recombinant protein was used as immunogen. A rabbit polyclonal antibody α-SWC4 was generated at the antibody production facilities from Physiologie et Génétique Moléculaire, Faculté des Sciences Ain-Chock (Casablanca Morroco).

Protein-binding microarrays

To determine SWC4 DNA-binding specificity, a translational fusion to Maltose Binding Protein (MBP) was obtained. Coding sequence of SWC4 was cloned into pDNONR201 and then mobilized into pDEST-TH1 to obtain a MBP-SCW4 fusion. This construct was then transformed into BL21 *E.coli* strain and recombinant protein synthesis was induced with 1 mM IPTG, following standard procedures. 25 mL of an induced culture were pelleted and used for incubation of the protein binding microarray (PBM) as described (Godoy et al., 2011; Franco-Zorrilla et al., 2014).

The PBMs represent all possible 11-mer double-stranded sequence combinations, as well as lower order k-mers, compacted in a microarray slide containing ~170 k oligonucleotide probes. This design is particularly suitable for the analysis of eukaryotic DNA-binding proteins given the large number of oligonucleotide probes. In average, any non-palindromic and palindromic 8-mer is contained in 250 and 125 oligonucleotide probes, respectively. A soluble protein extract from the pelleted induced *E. coli* culture was obtained as in Godoy et al. (2011) and incubated with the double stranded PBM for 2.5 hours at room temperature to allow DNA-protein interactions. DNA–protein complexes were detected with sequential incubations with primary rabbit polyclonal antibody to MBP (Abcam, http://www.abcam.com/) for 16 hours at room temperature and goat anti-rabbit IgG DyLight 549 conjugated (Pierce, http://www.piercenet.com/) in phosphate buffered saline (PBS)–2% milk for 3 h at room temperature. Slide incubations and washes were performed as described (Godoy et al., 2011; Franco-Zorrilla et al., 2014).

PBM was scanned in a DNA Microarray Scanner at 5 μm resolution and quantified with Feature Extraction 9.0 software (Agilent Technologies) as in Franco-Zorrilla et al. (2014). Normalization of probe intensities, extraction of probe signal intensities and calculation of enrichment scores (E-scores) and Z-scores of all the possible 8-

mers were carried out with the PBM Analysis Suite (Berger and Bulyk, 2009) with Perl scripts modified to adapt them to PBM dimensions and input files generated by Feature Extraction software. E-score is a rank-based, non-parametric measure of binding affinity ranging from -0.5 (reflecting no binding to DNA) to +0.5, representing the maximum theoretical affinity for a given 8-mer (Berger et al., 2006). As a general rule, E-scores above 0.42 denote specific binding of the protein to DNA (Berger et al., 2006). Similarly, Z-scores provide an additional statistical measure of binding affinity, as the bigger the Z-score, the higher the binding to DNA. In the experiment shown in this work, the Z-scores of the 8-mer motifs recognized with the highest affinities by SCW4 range from 5.6 to 4, which correspond to probabilities due to chance from approximately 1e-8 to 3e-5, respectively.

Electrophoretic mobility shift assay (EMSA)

Three different AT-rich probes and one GC-rich were used in EMSA assays (Hellman and Fried, 2007): 'AT-1', 'AT-2' and 'AT-3' correspond to 8-mer motifs ranked at positions 1, 2 and 4 respectively in PBM assay; whereas the 'GC' sequence corresponds to the 8-mer motif ranked at the lowest position in PBM assay. Double stranded biotinylated probes were obtained by amplification with the following oligonucleotides AT-1: 5'-GATCCTCTCGCGTACTAAGTCTATAATTAAATTATTTAAGCGTAGCGTATGCGTA; AT-2: 5'-GATCCTCTCGCGTACTAAGTCTATAAATAAAATATTTAAGCGTAGCGTATGCGTA; AT-3: 5'-GATCCTCTCGCGTACTAAGTCTATTTAATTAATATTTAAGCGTAGCGTATGCGTA; GC: 5'-GATCCTCTCGCGTACTAAGTCTATAGCCCCCGTATTTAAGCGTAGCGTATGCGTA (variable sequence motifs underlined). Amplifications were performed with biotinylated oligonucleotides Bio-5′-GATCCTCTCGCGTAC-3′ and Bio-5′-TACGCATACGCTACG-3′, or without biotynilation in the case of the 'cold' AT-1 probe. Binding reactions were performed with 50 or 100 ng of purified SCW4-MBP protein and 20 ng of biotinylated probes for 45 min at 4ºC in 10 mM Tris pH 7.5, 50

mM KCl, 1 mM DTT, 10 mM MgCl2, 2.5% glycerol and 1 υg poly dIdC, resolved in 5% PAGE and transferred to nylon Biodyne membrane. Detection of biotin was performed with LightShift Chemiluminescent EMSA kit (Thermo Scientific).

References for Supplemental Methods

Bonzon-Kulichenko, E., Garcia-Marques, F., Trevisan-Herraz, M., and Vazquez, J. (2014). Revisiting Peptide identification by high-accuracy mass spectrometry: problems associated with the use of narrow mass precursor windows. J Proteome Res **14,** 700-710.

Bonzon-Kulichenko, E., Perez-Hernandez, D., Nunez, E., Martinez-Acedo, P., Navarro, P., Trevisan-Herraz, M., Ramos Mdel, C., Sierra, S., Martinez-Martinez, S., Ruiz-Meana, M., Miro-Casas, E., Garcia-Dorado, D., Redondo, J.M., Burgos, J.S., and Vazquez, J. (2011). A robust method for quantitative high-throughput analysis of proteomes by 18O labeling. Mol Cell Proteomics **10,** M110 003335.

Franco-Zorrilla, J.M., Lopez-Vidriero, I., Carrasco, J.L., Godoy, M., Vera, P., and Solano, R. (2014). DNA-binding specificities of plant transcription factors and their potential to define target genes. Proc Natl Acad Sci U S A **111,** 2367-2372.

Godoy, M., Franco-Zorrilla, J.M., Perez-Perez, J., Oliveros, J.C., Lorenzo, O., and Solano, R. (2011). Improved protein-binding microarrays for the identification of DNA-binding specificities of transcription factors. Plant J **66,** 700-711.

Hellman, L.M., and Fried, M.G. (2007). Electrophoretic mobility shift assay (EMSA) for detecting protein-nucleic acid interactions. Nat Protoc **2,** 1849-1861.

Jorge, I., Burillo, E., Mesa, R., Baila-Rueda, L., Moreno, M., Trevisan-Herraz, M., Silla-Castro, J.C., Camafeita, E., Ortega-Munoz, M., Bonzon-Kulichenko, E., Calvo, I., Cenarro, A., Civeira, F., and Vazquez, J. (2014). The human HDL proteome displays high inter-individual variability and is altered dynamically in response to angioplasty-induced atheroma plaque rupture. J Proteomics **106,** 61-73.

Lazaro, A., Valverde, F., Pineiro, M., and Jarillo, J.A. (2012). The Arabidopsis E3 ubiquitin ligase HOS1 negatively regulates CONSTANS abundance in the photoperiodic control of flowering. Plant Cell **24,** 982-999.

Martinez-Bartolome, S., Navarro, P., Martin-Maroto, F., Lopez-Ferrer, D., Ramos-Fernandez, A., Villar, M., Garcia-Ruiz, J.P., and Vazquez, J. (2008). Properties of average score distributions of SEQUEST: the probability ratio method. Mol Cell Proteomics **7,** 1135-1145.

Navarro, P., Trevisan-Herraz, M., Bonzon-Kulichenko, E., Nunez, E., Martinez-Acedo, P., Perez-Hernandez, D., Jorge, I., Mesa, R., Calvo, E., Carrascal, M., Hernaez, M.L., Garcia, F., Barcena, J.A., Ashman, K., Abian, J., Gil, C., Redondo, J.M., and Vazquez, J. (2014). General statistical framework for quantitative proteomics by stable isotope labeling. J Proteome Res **13,** 1234-1247.

SUPPLEMENTAL DATA SET LEGENDS

Supplemental Data Set 1. *Arabidopsis* SWC6 interactors. SWC6-Myc immunoprecipitation and mass spectrometry analysis were performed with protein extracts from 10 day-old seedlings. The number of identified peptides in c-Myc eluates and in the agarose beads samples from SWC6-Myc and non-tagged control seedlings were compared. The table only shows the protein hits that were identified in the SWC6-Myc sample in both experiments but not in any of the control c-Myc peptide eluates. SWC4 is highlighted in blue.

Supplemental Data Set 2. RNA-seq data. File list showing the differentially expressed genes (DEG) in *swc4i* compared to WT determined by DESeq2 analysis (p<0.05); Fold-change expression is represented as $\log_2$ Ratio (*swc4i*/Col); FDR is for False Discovery Rate.

Supplemental Data Set 3. HTA9 ChIP-seq data. File list showing the list of genes with a peak of HTA9 in *swc4i* and WT, and a list of genes with reduced levels of HTA9 in *swc4i* compared to WT determined by SICER analysis.

Supplemental Data Set 4. Overlap between RNAseq and ChIP-seq data. File list showing genes upregulated and with low HTA9 levels in *swc4i*, and the list of the 34 transcription factors upregulated and with low HTA9 levels in *swc4i*.

Supplemental Data Set 5. Depicted location of PCR amplicons of SWC4 ChIP binding sites and the AT-rich motifs recognized by SWC4 in *FT*, *FUL*, *IAA19* and *ERF9* genomic regions (matrix-scan RSAT tool; markov order 1; p< 0.01).